Steel and Composite Structures, *Vol. 35, No. 1* (*2020*) *1-12*
DOI: https://doi.org/10.12989/scs.2020.35.1.001

Buckling response of smart plates reinforced by nanoparticles utilizing analytical method

Ahmad Farrokhian*

Mechanical Engineering group, Pardis College, Isfahan University of Technology, Isfahan 84156-83111, Iran

(*Received January 25, 2020, Revised March 12, 2020, Accepted March 19, 2020*)

Abstract. This article deals with the buckling analysis in the plates containing carbon nanotubes (CNTs) subject to axial load. In order to control the plate smartly, a piezoelectric layer covered the plate. The plate is located in elastic medium which is modeled by spring elements. The Mori-Tanaka low is utilized for calculating the equivalent mechanical characteristics of the plate. The structure is modeled by a thick plate and the governing equations are deduced using Hamilton's principle under the assumption of higher-order shear deformation theory (HSDT). The Navier method is applied to obtain the bulking load. The effects of the applied voltage to the smart layer, agglomeration and volume percent of CNT nanoparticles, geometrical parameters and elastic medium of the structure are assessed on the buckling response. It has been demonstrated that by applying a negative voltage, the buckling load is increased significantly.

Keywords: smart plate; buckling load; piezoelectric layer; elastic medium; analytical method

1. Introduction

The sandwich structures are used recently in many industries due to achieve the excellent material properties. One of the novel ways for control the important structure is utilizing piezoelectric layer as sensor and actuator. On the other hands, FGMs are used in many works due to high temperature resistance and good mechanical characteristics. In this paper, we used a FGM cylinder integrated by two piezoelectric layer and our purpose is studding the stress response and electric potential of the structure.

Stress response of the structures is presented by many authors. An exact solution for axisymmetric problem of an infinitely long, radially polarized, radially orthotropic piezoelectric hollow circular cylinder rotating about its axis at constant angular velocity was developed by Galic and Horgan (2002). Liew *et al*. (2003) investigated thermal stress behavior of FGM hollow circular cylinders. The analytical solution of a FGM piezo-thermo-elastic hollow cylinder was studied by Chen and Shi (2005). Dai *et al.* (2006) investigated analytical solutions for FGM cylinder subjected to uniform magnetic field. Lee (2007) studied three-dimensional analysis of stress distribution in a long circular cylinder containing an elliptical crack. Based on the surface/interface elasticity theory, the effect of surface/interface on the dynamic stress of two interacting cylindrical nano-inhomogeneities under compressional waves was considered by Fang *et al.* (2010). Li *et al.* (2012) investigated thermal stress analysis and structure optimum of the neck tube support system of cryogenic cylinders subjected to internal pressure. Thermoelastic stress analysis of the contact between a flat plate and a cylinder was studied by Garinei and Marsili (2013). Sallem and Hamdi (2015) presented experimental measurements of ground work piece obtained by X-Ray diffraction show high level of compressive residual stresses generated in ground surfaces. A cross-section analysis technique that provides interaction curves of arbitrary welded sections with consideration of the effects of residual stress by meshing the entire section into small triangular fibers was formulated. by Li *et al*. (2015). Numerical analysis of large amplitude free vibration behaviour of laminated composite spherical shell panel embedded with the piezoelectric layer was presented by Singh and Panda (2015a). The nonlinear free vibration behaviour of laminated composite single/doubly curved shell panel embedded with the piezoelectric layer was investigated numerically by Singh and Panda (2015a). Singh and Panda (2016) investigated the geometrical nonlinear free vibration characteristic of cylindrical composite shell panel embedded with piezoelectric layers. The geometrically nonlinear transient response of the smart laminated composite plate was investigated by Singh *et al.* (2016a) under the coupled electromechanical load. Singh *et al.* (2016b) studied geometrical nonlinear flexural behaviour of laminated composite shell panels integrated with the piezoelectric fibre reinforced composite (PFRC) layer. Benchiha *et al*. (2016) used the stress intensity factor (SIF) and crack opening displacement (COD) for cracks repaired with single and double-sided composite patches. An analytical sandwich beam model and its corresponding beam finite element model for geometric and material nonlinear analysis were developed by Chen *et al.* (2016). The flexural behaviour of the laminated composite plate embedded with two different smart materials (piezoelectric and magnetostrictive) and subsequent deflection suppression were investigated by Dutta *et al*. (2017). Static

*Corresponding author, Ph.D.
E-mail: ahmadfarrokhian@yahoo.com

http://www.techno-press.org/?journal=scs&subpage=8
ISSN: 1229-9367 (Print), 1598-6233 (Online)

bending and strength behaviour of the laminated composite plate embedded with magnetostrictive (MS) material was computed numerically by Suman *et al*. (2017). A layerwise (LW) formulation based on the Galerkin method was presented by Ahmadi (2017) to investigate the three-dimensional stress state in long sandwich plate which is subjected to tension force and pure bending moment. The eigenfrequency responses of a nanoplate structure were evaluated numerically by Mehr *et al.* (2018) via a novel higher-order mathematical model and finite-element method including nonlocal elasticity theory. Thermal buckling temperature values of the graded carbon nanotube reinforced composite shell structure was explored by Mehar and panda (2019). Wang and Shao (2018) used theoretical analysis and experimental tests for new I-girder to investigate the stress distribution in the flanges and in the corrugated web. Chaabane *et al*. (2019) presented static and dynamic behaviors of functionally graded beams (FGB) is presented using a hyperbolic shear deformation theory. Boulefrakh *et al.* (2019) presented a simple quasi 3D hyperbolic shear deformation model for bending and dynamic behavior of functionally graded (FG) plates resting on visco-Pasternak foundations. Zaoui *et al*. (2019) studied free vibration of functionally graded plates on elastic foundations. Karami *et al*. (2019) studied size-dependent wave propagation analysis of functionally graded (FG) anisotropic nanoplates based on a nonlocal strain gradient refined plate model. Habib *et al.* (2019) represents a mathematical analysis of the stresses and strains of an FGM cylinder. Boukhlif *et al.* (2019) studied a dynamic investigation of functionally graded (FG) plates resting on elastic foundation using a simple quasi-3D higher shear deformation theory. Addou *et al.* (2019) investigated the effect of Winkler/Pasternak/Kerr foundation and porosity on dynamic behavior of FG plates using a simple quasi-3D hyperbolic theory. Semmah *et al*. (2019) investigated the thermal buckling characteristics of zigzag single-walled boron nitride (SWBNNT) embedded in a one-parameter elastic medium. Mahmoudi *et al.* (2019) applied a refined quasi-three-dimensional shear deformation theory for thermo-mechanical analysis of functionally graded sandwich plates. Doan *et al.* (2020) presented the stress concentration phenomenon at the points with force jumping, structural jumping and sudden changes of boundary conditions of cylinder laminated shells. Kaddari *et al.* (2020) studied structural behaviour of functionally graded porous plates on elastic foundation using a new quasi-3D model.

In the present study, buckling of smart plate containing CNT resting on the elastic medium is investigated. The structure is covered by a piezoelectric layer subjected to the external voltage. On the basis of HSDT, the governing equations are inferred utilizing Hamilton's principal. Navier method is adopted to determine buckling load. The influence of applied voltage to the smart layer, agglomeration and volume percent of CNTs, geometrical parameters and elastic medium are shown on the buckling load.

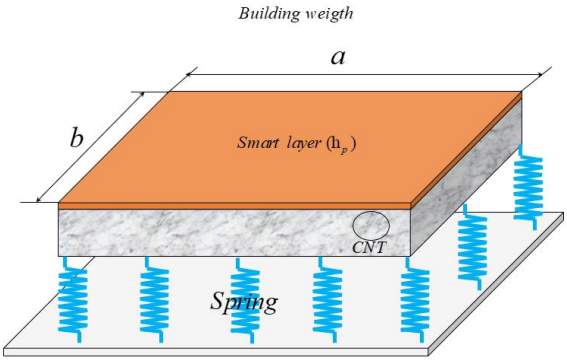

Fig. 1 A schematic configuration of pad concrete plate containing nanoparticles covered by smart layer resting on elastic medium

2. Formulation

In Fig. 1, a plate is shown with length, width, thickness of a, b and h_c, respectively. The structure is mixed by CNT nanoparticles and covered by a piezoelectric layer with a thickness of h_p. In addition, the plate is located at the elastic medium which is modeled by the spring element.

There are many theories for modelling of structures (El-Haina 2017, Menasria 2017, Chikh 2017, Bouafia 2017, Besseghier 2017, Bellifa 2017, Mouffoki 2017, Khetir 2017, Abualnour *et al.* (2019), Draiche *et al*. (2019), Belbachir *et al.* (2019), Medani *et al.* (2019), Sahla *et al.* (2019)). Based on the HSDT thick plate theory, the displacement field is (Reddy 2002)

$$u_1(x,y,z,t)=u(x,y,t)+z\,\phi_x(x,y,t)+c_1 z^3\left(\phi_x+\frac{\partial w}{\partial x}\right), \quad (1)$$

$$u_2(x,y,z,t)=v(x,y,t)+z\,\phi_y(x,y,t)+c_1 z^3\left(\phi_y+\frac{\partial w}{\partial y}\right), \quad (2)$$

$$u_3(x,y,z,t)=w(x,y,t), \quad (3)$$

The mid-plane displacements are u, v and w along the x, y, z directions, correspondingly; ϕ_x and φ_y present the rotational displacement about x and y directions, correspondingly. Utilizing the above relations, the relations between the strains and displacements are

$$\begin{pmatrix}\varepsilon_{xx}\\ \varepsilon_{yy}\\ \gamma_{xy}\end{pmatrix}=\begin{pmatrix}\varepsilon^0_{xx}\\ \varepsilon^0_{yy}\\ \gamma^0_{xy}\end{pmatrix}+z\begin{pmatrix}\varepsilon^1_{xx}\\ \varepsilon^1_{yy}\\ \gamma^1_{xy}\end{pmatrix}+z^3\begin{pmatrix}\varepsilon^3_{xx}\\ \varepsilon^3_{yy}\\ \gamma^3_{xy}\end{pmatrix}, \quad (4)$$

$$\begin{pmatrix}\gamma_{yz}\\ \gamma_{xz}\end{pmatrix}=\begin{pmatrix}\gamma^0_{yz}\\ \gamma^0_{xz}\end{pmatrix}+z^2\begin{pmatrix}\gamma^2_{yz}\\ \gamma^2_{xz}\end{pmatrix}, \quad (5)$$

where

$$\begin{pmatrix}\varepsilon_{xx}^0\\ \varepsilon_{yy}^0\\ \gamma_{xy}^0\end{pmatrix}=\begin{pmatrix}\dfrac{\partial u}{\partial x}\\ \dfrac{\partial v}{\partial y}\\ \dfrac{\partial u}{\partial y}+\dfrac{\partial v}{\partial x}\end{pmatrix},\quad \begin{pmatrix}\varepsilon_{xx}^1\\ \varepsilon_{yy}^1\\ \gamma_{xy}^1\end{pmatrix}=\begin{pmatrix}\dfrac{\partial \varphi_x}{\partial x}\\ \dfrac{\partial \varphi_y}{\partial y}\\ \dfrac{\partial \varphi_x}{\partial y}+\dfrac{\partial \varphi_y}{\partial x}\end{pmatrix},$$

$$\begin{pmatrix}\varepsilon_{xx}^3\\ \varepsilon_{yy}^3\\ \gamma_{xy}^3\end{pmatrix}=c_1\begin{pmatrix}\dfrac{\partial \varphi_x}{\partial x}+\dfrac{\partial^2 w}{\partial x^2}\\ \dfrac{\partial \varphi_y}{\partial y}+\dfrac{\partial^2 w}{\partial y^2}\\ \dfrac{\partial \varphi_x}{\partial y}+\dfrac{\partial \varphi_y}{\partial x}+2\dfrac{\partial^2 w}{\partial x\,\partial y}\end{pmatrix}, \tag{6a}$$

$$\begin{pmatrix}\gamma_{yz}^0\\ \gamma_{xz}^0\end{pmatrix}=\begin{pmatrix}\phi_y+\dfrac{\partial w}{\partial y}\\ \phi_x+\dfrac{\partial w}{\partial x}\end{pmatrix},\quad \begin{pmatrix}\gamma_{yz}^2\\ \gamma_{xz}^2\end{pmatrix}=c_2\begin{pmatrix}\phi_y+\dfrac{\partial w}{\partial y}\\ \phi_x+\dfrac{\partial w}{\partial x}\end{pmatrix}, \tag{6b}$$

For the piezoelectric material, the stresses $\boldsymbol{\sigma}$ and strains $\boldsymbol{\varepsilon}$ are coupled by displacement related to electric $\mathbf{D}$ and by field $\mathbf{E}$ as follows (Tiersten 1969)

$$\begin{bmatrix}\sigma_{xx}\\ \sigma_{yy}\\ \sigma_{zz}\\ \tau_{yz}\\ \tau_{xz}\\ \tau_{xy}\end{bmatrix}=\begin{bmatrix}C_{11}&C_{12}&C_{13}&0&0&0\\ C_{12}&C_{22}&C_{23}&0&0&0\\ C_{13}&C_{23}&C_{33}&0&0&0\\ 0&0&0&C_{44}&0&0\\ 0&0&0&0&C_{55}&0\\ 0&0&0&0&0&C_{66}\end{bmatrix}\left(\begin{Bmatrix}\varepsilon_{xx}\\ \varepsilon_{yy}\\ \varepsilon_{zz}\\ \gamma_{yz}\\ \gamma_{xz}\\ \gamma_{xy}\end{Bmatrix}\right)-\begin{bmatrix}0&0&e_{31}\\ 0&0&e_{32}\\ 0&0&e_{33}\\ 0&e_{24}&0\\ e_{15}&0&0\\ 0&0&0\end{bmatrix}\begin{Bmatrix}E_x\\ E_y\\ E_z\end{Bmatrix} \tag{7}$$

$$\begin{bmatrix}D_x\\ D_y\\ D_z\end{bmatrix}=\begin{bmatrix}0&0&0&0&e_{15}&0\\ 0&0&0&e_{24}&0&0\\ e_{31}&e_{31}&e_{33}&0&0&0\end{bmatrix}\left(\begin{Bmatrix}\varepsilon_{xx}\\ \varepsilon_{yy}\\ \varepsilon_{zz}\\ \gamma_{yz}\\ \gamma_{xz}\\ \gamma_{xy}\end{Bmatrix}\right)+\begin{bmatrix}\in_{11}&0&0\\ 0&\in_{22}&0\\ 0&0&\in_{33}\end{bmatrix}\begin{Bmatrix}E_x\\ E_y\\ E_z\end{Bmatrix} \tag{8}$$

The elastic, dielectric and piezoelectric constants are indicated by C_{ij}, $\in_{ij}$ and e_{ij} respectively.

The electric field can be determined respect to the electric potential (Φ)

$$E_k=-\nabla\Phi, \tag{9}$$

Where the electric potential is considered consists of a linear variation and half-cosine (the Maxwell equation are satisfied) as

$$\Phi(x,y,z,t)=-\cos(\frac{\pi z}{h})\varphi(x,y,t)+\frac{2V_0 z}{h}, \tag{10}$$

where $\varphi(x,y,t)$ is the electric potential with satisfying the boundary conditions related to electric; V_0 is the external voltage. Based on Eqs. (4) and (5), the stress equations of the smart layer may be given as

$$\sigma_{xx}^p=C_{11}\varepsilon_{xx}+C_{12}\varepsilon_{yy}+e_{31}\left(\frac{\pi}{h}\sin\left(\frac{\pi z}{h}\right)\varphi+\frac{2V_0}{h}\right), \tag{11}$$

$$\sigma_{yy}^p=C_{12}\varepsilon_{xx}+C_{22}\varepsilon_{yy}+e_{32}\left(\frac{\pi}{h}\sin\left(\frac{\pi z}{h}\right)\varphi+\frac{2V_0}{h}\right), \tag{12}$$

$$\tau_{yz}^p=C_{44}\gamma_{yz}-e_{15}\left(\cos\left(\frac{\pi z}{h}\right)\frac{\partial\varphi}{\partial y}\right), \tag{13}$$

$$\tau_{xz}^p=C_{55}\gamma_{zx}-e_{24}\left(\cos\left(\frac{\pi z}{h}\right)\frac{\partial\varphi}{\partial x}\right), \tag{14}$$

$$\tau_{xy}^p=C_{66}\gamma_{xy}, \tag{15}$$

Utilizing Eqs. (4) and (6), the electric displacement equations of the piezoelectric layer are

$$D_x=e_{15}\gamma_{xz}+\in_{11}\left(\cos\left(\frac{\pi z}{h}\right)\frac{\partial\varphi}{\partial y}\right), \tag{16}$$

$$D_y=e_{24}\gamma_{zy}+\in_{22}\left(\cos\left(\frac{\pi z}{h}\right)\frac{\partial\varphi}{\partial y}\right), \tag{17}$$

$$D_z=e_{31}\varepsilon_{xx}+e_{32}\varepsilon_{yy}-\in_{33}\left(\frac{\pi}{h}\sin\left(\frac{\pi z}{h}\right)\varphi+\frac{2V_0}{h}\right). \tag{18}$$

For the plate, the stress relations can be given by neglecting piezoelectric constants of Eqs. (9)-(13) as

$$\sigma_{xx}^c=\underbrace{\frac{E}{1-\nu^2}}_{Q_{11}}\varepsilon_{xx}+\underbrace{\frac{E\nu}{1-\nu^2}}_{Q_{12}}\varepsilon_{yy}, \tag{19}$$

$$\sigma_{yy}^c=\underbrace{\frac{E\nu}{1-\nu^2}}_{Q_{12}}\varepsilon_{xx}+\underbrace{\frac{E}{1-\nu^2}}_{Q_{22}}\varepsilon_{yy}, \tag{20}$$

$$\tau_{yz}^c=\underbrace{\frac{E}{2(1+\nu)}}_{Q_{44}}\gamma_{yz}, \tag{21}$$

$$\tau_{xz}^c=\underbrace{\frac{E}{2(1+\nu)}}_{Q_{55}}\gamma_{zx}, \tag{22}$$

$$\tau_{xy}^c=\underbrace{\frac{E}{2(1+\nu)}}_{Q_{66}}\gamma_{xy}, \tag{23}$$

where the modulus of elasticity (E) and Poisson's ratio (ν) based on the Mori-Tanaka model (Shi and Feng 2004) may be given as

$$E=\frac{9KG}{3K+G}\quad , \tag{24}$$

$$\upsilon=\frac{3K-2G}{6K+2G}. \tag{25}$$

in which the equivalent shear modulus (G) and bulk modulus (K) are presented in Appendix A.

2.4 Energy method

The potential energy related to pad concrete plate with a smart layer can be expressed as

$$U=\frac{1}{2}\int\begin{pmatrix}\sigma_{xx}^{c}\varepsilon_{xx}+\sigma_{yy}^{c}\varepsilon_{yy}+\tau_{xz}^{c}\gamma_{xz}+\tau_{yz}^{c}\gamma_{yz}\\+\tau_{xy}^{c}\gamma_{xy}+\sigma_{xx}^{p}\varepsilon_{xx}+\sigma_{yy}^{p}\varepsilon_{yy}+\tau_{xz}^{p}\gamma_{xz}\\+\tau_{yz}^{p}\gamma_{yz}+\tau_{xy}^{p}\gamma_{xy}\\-D_xE_x-D_yE_y-D_zE_z\end{pmatrix}dV\ , \tag{26}$$

Substituting Eqs. (4), (7) and (8) into Eq. (24) yields

$$\begin{aligned}U=&\frac{1}{2}\int\left(N_{xx}\left(\frac{\partial u}{\partial x}\right)+N_{yy}\left(\frac{\partial v}{\partial y}\right)+Q_{yy}\left(\frac{\partial w}{\partial y}+\phi_y\right)\right.\\&+Q_{xx}\left(\frac{\partial w}{\partial x}+\phi_x\right)+N_{xy}\left(\frac{\partial v}{\partial x}+\frac{\partial u}{\partial y}\right)+M_{xx}\frac{\partial\phi_x}{\partial x}\\&+M_{yy}\frac{\partial\phi_y}{\partial y}+M_{xy}\left(\frac{\partial\phi_x}{\partial y}+\frac{\partial\phi_y}{\partial x}\right)+K_{yy}\left(c_2\left(\phi_y+\frac{\partial w}{\partial y}\right)\right)\\&+K_{xx}\left(c_2\left(\phi_x+\frac{\partial w}{\partial x}\right)\right)+P_{xx}\left(c_1\left(\frac{\partial\phi_x}{\partial x}+\frac{\partial^2 w}{\partial x^2}\right)\right)\\&+P_{yy}\left(c_1\left(\frac{\partial\phi_y}{\partial y}+\frac{\partial^2 w}{\partial y^2}\right)\right)+P_{xy}\left(\frac{\partial\phi_y}{\partial x}+\frac{\partial\phi_x}{\partial y}+2\frac{\partial^2 w}{\partial x\,\partial y}\right)\Bigg)dA\\&+\int_{-h/2}^{h/2+h_p}\int_0^{2\pi}\int_0^{L}-D_x\left[\cos\left(\frac{\pi z}{h}\right)\frac{\partial\varphi}{\partial x}\right]-D_y\left[\cos\left(\frac{\pi z}{h}\right)\frac{\partial\varphi}{\partial y}\right]\\&\left.-D_z\left[-\frac{\pi}{h}\sin\left(\frac{\pi z}{h}\right)\varphi-\frac{2V_0}{h}\right]\right\}dxdydz\ ,\end{aligned} \tag{27}$$

where the resultant may be given as

$$\begin{Bmatrix}N_{xx}\\N_{yy}\\N_{xy}\end{Bmatrix}=\int_{-\frac{h_c}{2}}^{\frac{h_c}{2}}\begin{Bmatrix}\sigma_{xx}^{c}\\\sigma_{yy}^{c}\\\tau_{xy}^{c}\end{Bmatrix}dz+\int_{\frac{h_c}{2}}^{\frac{h_c}{2}+h_p}\begin{Bmatrix}\sigma_{xx}^{p}\\\sigma_{yy}^{p}\\\tau_{xy}^{p}\end{Bmatrix}dz \tag{28}$$

$$\begin{Bmatrix}Q_x\\Q_y\end{Bmatrix}=\int_{-\frac{h_c}{2}}^{\frac{h_c}{2}}\begin{Bmatrix}\tau_{xz}^{c}\\\tau_{yz}^{c}\end{Bmatrix}dz+\int_{-\frac{h_c}{2}}^{\frac{h_c}{2}+h_p}\begin{Bmatrix}\tau_{xz}^{p}\\\tau_{yz}^{p}\end{Bmatrix}dz\ , \tag{29}$$

$$\begin{Bmatrix}M_{xx}\\M_{yy}\\M_{xy}\end{Bmatrix}=\int_{-\frac{h_c}{2}}^{\frac{h_c}{2}}\begin{Bmatrix}\sigma_{xx}^{c}\\\sigma_{yy}^{c}\\\tau_{xy}^{c}\end{Bmatrix}z^2dz+\int_{\frac{h_c}{2}}^{\frac{h_c}{2}+h_p}\begin{Bmatrix}\sigma_{xx}^{p}\\\sigma_{yy}^{p}\\\tau_{xy}^{p}\end{Bmatrix}z^2dz\ , \tag{30}$$

$$\begin{Bmatrix}P_{xx}\\P_{yy}\\P_{xy}\end{Bmatrix}=\int_{-\frac{h_c}{2}}^{\frac{h_c}{2}}\begin{Bmatrix}\sigma_{xx}^{c}\\\sigma_{yy}^{c}\\\tau_{xy}^{c}\end{Bmatrix}z^3dz+\int_{\frac{h_c}{2}}^{\frac{h_c}{2}+h_p}\begin{Bmatrix}\sigma_{xx}^{p}\\\sigma_{yy}^{p}\\\tau_{xy}^{p}\end{Bmatrix}z^3dz\ , \tag{31}$$

$$\begin{Bmatrix}K_x\\K_y\end{Bmatrix}=\int_{-\frac{h_c}{2}}^{\frac{h_c}{2}}\begin{Bmatrix}\tau_{xz}^{c}\\\tau_{yz}^{c}\end{Bmatrix}z^2dz+\int_{-\frac{h_c}{2}}^{\frac{h_c}{2}+h_p}\begin{Bmatrix}\tau_{xz}^{p}\\\tau_{yz}^{p}\end{Bmatrix}z^2dz\ , \tag{32}$$

The kinetic energy related to the smart concrete structure is

$$K=\frac{\left(\rho^c+\rho^p\right)}{2}\int\left(\dot{u}_1^{\,2}+\dot{u}_2^{\,2}+\dot{u}_3^{\,2}\right)dV\ , \tag{33}$$

where ρ^c and ρ^p are density of concrete and smart layer, respectively.

The external work due to elastic medium is

$$W_e=\int_0^{2\pi}\int_0^{L}[-K_sw\,]wdA, \tag{34}$$

where K_s is elastic spring constant.

Hamilton's principle is adopted to infer the governing equations

$$\int_0^t(\delta U-\delta K-\delta W_e)dt=0. \tag{35}$$

Replacing the Eqs. (25), (31) and (32) into Eq. (33) and neglecting kinetic energy yields

$$\delta u:\frac{\partial N_{xx}}{\partial x}+\frac{\partial N_{xy}}{\partial y}=0, \tag{36}$$

$$\delta v:\frac{\partial N_{xy}}{\partial x}+\frac{\partial N_{yy}}{\partial y}=0, \tag{37}$$

$$\begin{aligned}\delta w:&\frac{\partial Q_{xx}}{\partial x}+\frac{\partial Q_{yy}}{\partial y}+c_2\left(\frac{\partial K_{xx}}{\partial x}+\frac{\partial K_{yy}}{\partial y}\right)+N_{xx}\frac{\partial^2 w}{\partial x^2}+N_{yy}\frac{\partial^2 w}{\partial y^2}\\&-c_1\left(\frac{\partial^2 P_{xx}}{\partial x^2}+2\frac{\partial^2 P_{xy}}{\partial x\,\partial y}+\frac{\partial^2 P_{yy}}{\partial y^2}\right)-K_sw=0,\end{aligned} \tag{38}$$

$$\delta\phi_x:\frac{\partial M_{xx}}{\partial x}+\frac{\partial M_{xy}}{\partial y}+c_1\left(\frac{\partial P_{xx}}{\partial x}+\frac{\partial P_{xy}}{\partial y}\right)-Q_{xx}-c_2K_{xx}=0, \tag{39}$$

$$\delta\phi_y:\frac{\partial M_{xy}}{\partial x}+\frac{\partial M_{yy}}{\partial y}+c_1\left(\frac{\partial P_{xy}}{\partial x}+\frac{\partial P_{yy}}{\partial y}\right)-Q_{yy}-c_2K_{yy}=0, \tag{40}$$

$$\begin{aligned}\delta\varphi:\ &\int_{-h/2}^{h/2}\left\{\cos\left(\frac{\pi z}{h}\right)\left[\frac{\partial D_x}{\partial x}\right]+\cos\left(\frac{\pi z}{h}\right)\left[\frac{\partial D_y}{\partial y}\right]\right.\\&\left.+\frac{\pi}{h}\sin\left(\frac{\pi z}{h}\right)\left[D_z\right]\right\}dz=0\end{aligned} \tag{41}$$

where the moment of inertias are

$$I_i=\int_{-h_c/2}^{h_c/2}\rho^c z^i\,dz+\int_{h_c/2}^{h_c/2+h_p}\rho^p z^i dz\ , \tag{42}$$

$$J_i=I_i-\frac{4}{3h^2}I_{i+2}\qquad(i=1,4), \tag{43}$$

$$K_2=I_2-\frac{8}{3h^2}I_4+\left(\frac{4}{3h^2}\right)^2I_6, \tag{44}$$

Substituting Eqs. (4)-(6) into Eqs. (26)-(28), the stress resultants may be expressed as written in Appendix B.

3. Analytical method

Based on Navier method for simply supported boundary condition, we have

$$u(x,y,t)=u_0\cos(\frac{n\pi x}{L})\sin(\frac{m\pi y}{b}), \quad (45)$$

$$v(x,y,t)=v_0\sin(\frac{n\pi x}{L})\cos(\frac{m\pi y}{b}), \quad (46)$$

$$w(x,y,t)=w_0\sin(\frac{n\pi x}{L})\sin(\frac{m\pi y}{b}), \quad (47)$$

$$\phi_x(x,y,t)=\psi_{x0}\cos(\frac{n\pi x}{L})\sin(\frac{m\pi y}{b}), \quad (48)$$

$$\phi_y(x,y,t)=\psi_{y0}\sin(\frac{n\pi x}{L})\cos(\frac{m\pi y}{b}), \quad (49)$$

$$\varphi(x,y,t)=\varphi_0\sin(\frac{n\pi x}{L})\cos(\frac{m\pi y}{b}), \quad (50)$$

where n and m are axial and lateral mode numbers, respectively. Substituting Eqs. (43)-(48) into Eqs. (34)-(39) yields

$$\begin{bmatrix} K_{11} & K_{12} & K_{13} & K_{14} & K_{15} & K_{16} \\ K_{21} & K_{22} & K_{23} & K_{24} & K_{25} & K_{26} \\ K_{31} & K_{32} & K_{33} & K_{34} & K_{35} & K_{36} \\ K_{41} & K_{42} & K_{43} & K_{44} & K_{45} & K_{46} \\ K_{51} & K_{52} & K_{53} & K_{54} & K_{55} & K_{56} \\ K_{61} & K_{62} & K_{63} & K_{64} & K_{65} & K_{66} \end{bmatrix} \begin{bmatrix} u_0 \\ v_0 \\ w_0 \\ \psi_{x0} \\ \psi_{y0} \\ \varphi_0 \end{bmatrix} = 0, \quad (51)$$

Finally, for calculating the buckling load, the determinant of matrix in Eq. (49) should be equal to zero.

4. Numerical results

For the parametric study, a plate with Poisson's ratio of $\nu_c = 0.3$ and elastic modulus of $E_c = 70\,GPa$ is assumed. The reinforcement is CNT density and Hill's constants reported in Motezaker and Kolahchi (2017). The smart layer is made from polyvinylidene fluoride (PVDF) in which the mechanical properties are expressed in Table 1 (Farokhian (2020)). In this paper, dimensionless buckling load is defined as $P = N_x/(E_c a)$.

In order to validate the present results, we neglected from the agglomerated CNTs as reinforcement, elastic medium and studied buckling of simply supported laminated plate. Considering the material properties the same as Matsunaga (2000), the buckling load is shown in Table 2. As can be seen, the present results are in good agreement with Noor (1975) based on 3D elasticity solution, Putcha and Reddy (1986) based on FSDT and Matsunaga (2000) based on HSDT.

Table 1 PVDF material properties

Properties	PVDF	
C_{11}	238.24	(GPa)
C_{12}	3.98	(GPa)
C_{22}	23.6	(GPa)
e_{11}	-0.135	(C/m^2)
e_{12}	-0.145	(C/m^2)
$\in_{11}$	1.1e-8	(C^2/Nm^2)

Table 2 Comparison of present work with the published papers

Solution	E_1/E_2	
	3	10
A	5.3044	9.7621
B	5.3991	9.9652
C	5.3208	9.7172
D	5.3918	9.8452
A	5.3255	9.9603
B	5.4093	10.1360
C	5.3348	9.9414
D	3.4011	9.9087

A: 3D elasticity solution, Noor (1975)
B: FSDT, Putcha and Reddy (1986)
C: HSDT, Matsunaga (2000)
D: Present work

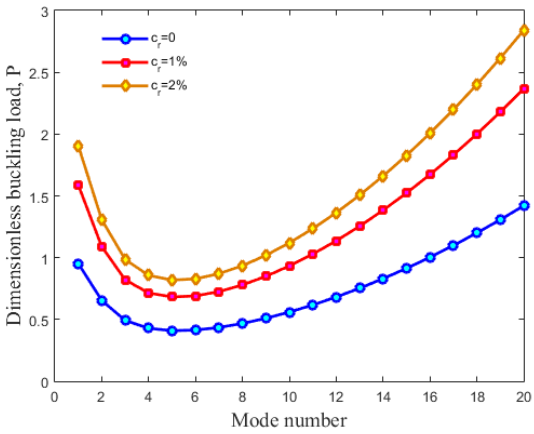

Fig. 2 The effect of CNT volume percent on the dimensionless buckling load

The dimensionless buckling load versus the axial mode number is shown in Fig. 2 for different CNT volume percent. It can be observed that the buckling load decreases

at first until reaches to the lowest amount and after that increasing process begins. The critical buckling load appears in the point where the buckling load is minimal. It may be concluded that with enhancing the CNT volume percent, the dimensionless buckling load enhances. It is due to the fact that with increasing CNT volume percent, the stiffness of the structure increases. In addition, the effect of CNT volume percent on the dimensionless buckling load becomes more prominent at higher axial mode numbers.

In order to show the effects of CNT agglomeration on the dimensionless buckling load, Fig. 3 is plotted. As can be seen, considering agglomeration effects leads to decrease in the dimensionless buckling load of the structure. It is because CNT agglomeration reduces the stability and rigidity of the structure.

Fig. 4 illustrates the effect of the applied external voltage on the dimensionless buckling load versus axial mode numbers. It can be concluded that the negative voltage increases the buckling load and positive one, the buckling load is reduced. It is because with negative voltage the structure is subjected to compressive load.

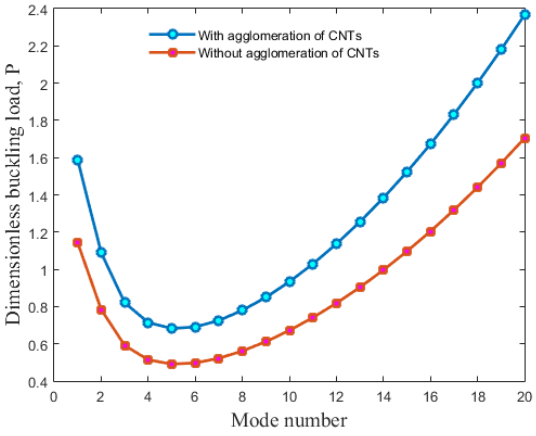

Fig. 3 The effect of CNT agglomeration on the dimensionless buckling load

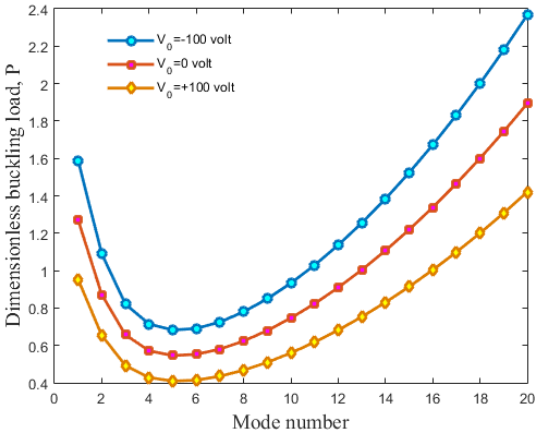

Fig. 4 The effect of external voltage on the dimensionless buckling load

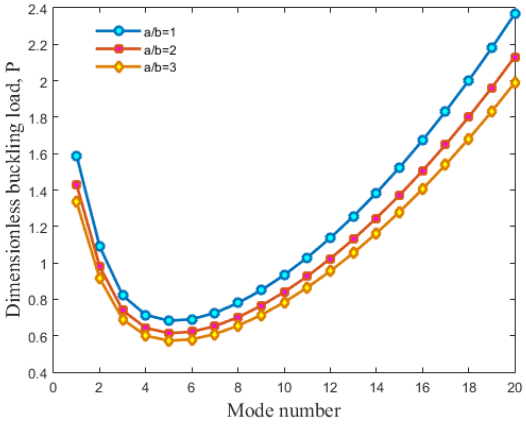

Fig. 5 The effect of length to width ratio of plate on the dimensionless buckling load

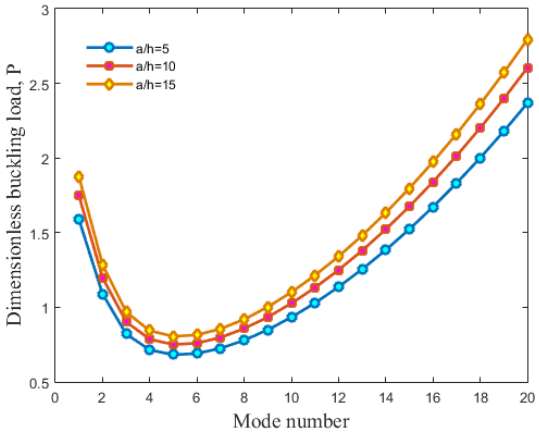

Fig. 6 The effect of length to total thickness ratio of plate on the dimensionless buckling load

The effect of length to width ratio of plate is presented in Fig 5 on the dimensionless buckling load versus axial mode number. It is found that with increasing the length to width ratio, the buckling load is reduced due to reduction in the stiffness of structure.

Fig. 6 demonstrates the effect of length to total thickness ratio of plate on the dimensionless buckling load versus axial mode number. As can be seen, with enhancing the length to total thickness ratio of plate, the buckling load is increased. It is physically due to this fact that with increasing the length to total thickness ratio of plate, the stiffness of structure increases.

The effect of the elastic medium is shown in Fig. 7 on the dimensionless buckling load versus axial mode number. It is found that the existence of the elastic medium increases the stiffness of the structure and thereby the dimensionless buckling load increases. It is since, the elastic foundation can increase the bending rigidity of the structure.

Fig. 8 demonstrates the effect of smart layer toplate thickness ratio of plate on the dimensionless buckling load versus axial mode number. As can be seen, with enhancing the smart layer to plate thickness ratio, the buckling load

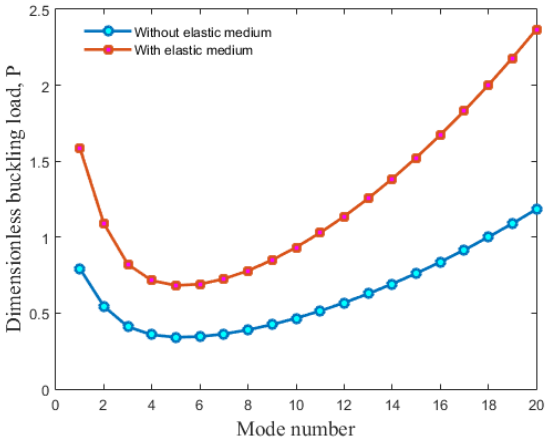

Fig. 7 The effect of elastic medium on the dimensionless buckling load

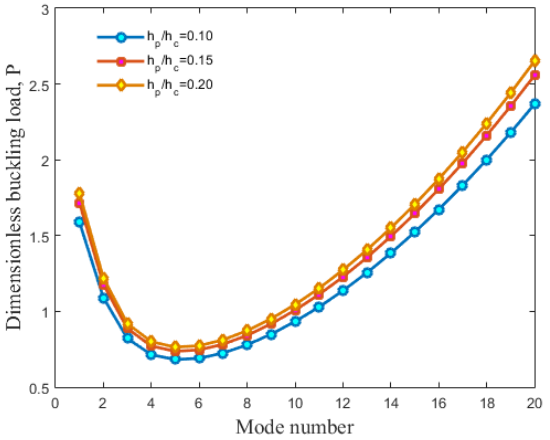

Fig. 8 The effect of length to total thickness ratio of plate on the dimensionless buckling load

decreases. It is physically due to this fact that with increasing smart layer to plate thickness ratio, the stiffness of structure decreases.

5. Conclusions

Buckling analysis in plate containing CNT with a smart layer was presented in this research based on mathematical modeling. The Mori-Tanaka model was applied for modeling the CNT in the plate. The governing equations were deduced by HSDT and Hamilton's principle. The analytical method was used to calculate the buckling load of the structure. The influence of the applied voltage, CNT volume fraction and agglomeration, elastic medium and geometrical parameters of the plate were assessed. Results show that:

- With enhancing the CNT volume percent, the dimensionless buckling load enhances.
- Considering agglomeration effects leads to decrease in the dimensionless buckling load of the structure.
- Tthe negative voltage increases the buckling load and positive one, the buckling load was reduced.
- With increasing the length to width ratio, the buckling load was reduced.
- With enhancing the length to total thickness ratio of plate, the buckling load was increased.
- With enhancing the smart layer to plate thickness ratio, the buckling load decreases.

References

Abualnour, M., Chikh, A., Hebali, H., Kaci, A., Tounsi. A., Bousahla, A.A. and Tounsi, A. (2019), "Thermomechanical analysis of antisymmetric laminated reinforced composite plates using a new four variable trigonometric refined plate theory", *Comput. Concrete,* **24**(6), 489-498. https://doi.org/10.12989/cac.2019.24.6.489.

Addou, F.Y., Meradjah, M., Bousahla, A.A., Benachour, A., Bourada, F., Tounsi, A. and Mahmoud, S.R. (2019), "Influences of porosity on dynamic response of FG plates resting on Winkler/Pasternak/Kerr foundation using quasi 3D HSDT", *Comput. Concrete,* **24**(4), 347-367. https://doi.org/10.12989/cac.2019.24.4.347.

Ahmadi, I. (2017), "A Galerkin Layerwise Formulation for three-dimensional stress analysis in long sandwich plates", *Steel Compos. Struct.,* **24**(5), 523-536. https://doi.org/10.12989/scs.2017.24.5.523.

Benchiha, A., Madani, K., Touzain, S., Feaugas, X. and Ratwani, M. (2016), "Numerical analysis of the Influence of the presence of disbond region in adhesive layer on the stress intensity factors (SIF) and crack opening displacement (COD) in plates repaired with a composite patch ", *Steel Compos. Struct.,* **20**(4), 951-962. https://doi.org/10.12989/scs.2016.20.4.951.

Bellifa, H., Benrahou, K.H., Bousahla, A.A., Tounsi, A. and Mahmoud, S.R. (2017), "A nonlocal zeroth-order shear deformation theory for nonlinear postbuckling of nanobeams", *Struct. Eng. Mech.,* **62**(6), 695-702. https://doi.org/10.12989/sem.2017.62.6.695.

Besseghier, A., Houari, M.S.A., Tounsi, A. and Hassan, S. (2017), "Free vibration analysis of embedded nanosize FG plates using a new nonlocal trigonometric shear deformation theory", *Smart Struct. Syst.*, **19**(6), 601-614. https://doi.org/10.12989/sss.2017.19.6.601.

Belbachir, N., Draich, K., Bousahla, A.A., Bourada, M., Tounsi, A. and Mohammadimehr, M. (2019), "Bending analysis of anti-symmetric cross-ply laminated plates under nonlinear thermal and mechanical loadings", *Steel Compos. Struct.*, **33**(1), 913-924. https://doi.org/10.12989/scs.2019.33.1.081.

Bouafia, K.h., Kaci, A., Houari M.S.A. and Tounsi, A. (2017), "A nonlocal quasi-3D theory for bending and free flexural vibration behaviors of functionally graded nanobeams", *Smart Struct. Syst.*, **19**(2), 115-126. https://doi.org/10.12989/sss.2017.19.2.115.

Boukhlif, Z., Bouremana, M., Bourada, F., Bousahla, A.A., Bourada, M., Tounsi, A. and Al-Osta, M.A. (2019), "A simple quasi-3D HSDT for the dynamics analysis of FG thick plate on elastic foundation", *Steel Compos. Struct.*, **31**(5), 503-516.: https://doi.org/10.12989/scs.2019.31.5.503.

Boulefrakh, L., Hebali, H., Chikh, A., Bousahla, A.A., Tounsi, A. and Mahmoud, S.R. (2019), "The effect of parameters of visco-Pasternak foundation on the bending and vibration properties of

a thick FG plate", *Geomech. Eng.*, **18**(2), 161-178. https://doi.org/10.12989/gae.2019.18.2.161.

Chaabane, L.A., Bourada, F., Sekkal, M., Zerouati, S., Zaoui, F.Z., Tounsi, A., Derras, A., Bousahla, A.A. and Tounsi, A. (2019), "Analytical study of bending and free vibration responses of functionally graded beams resting on elastic foundation", *Struct. Eng. Mech.*, **71**(2), 185-196. https://doi.org/10.12989/sem.2019.71.2.185.

Chikh, A., Tounsi, A., Hebali, H. and Mahmoud, S.R. (2017), "Thermal buckling analysis of cross-ply laminated plates using a simplified HSDT", *Smart Struct. Syst.*, **19**(3), 289-297. https://doi.org/10.12989/sss.2017.19.3.289.

Chen, Y. and Shi, Z.F. (2005), "Analysis of a functionally graded piezothermoelatic hollow cylinder", *J. Zhejiang Univ. SCI.,* **6A**, 956–61, https://doi.org/10.1080/01495730802250508.

Chen, X.Ch., Bai, Z.zh., Zeng, Y., Jiang, R.J. and Francis, T.K. (2016), "Prestressed concrete bridges with corrugated steel webs: Nonlinear analysis and experimental investigation", *Steel Compos. Struct.*, **21**(5), 1045-1067. https://doi.org/10.12989/scs.2016.21.5.1045.

Draiche, K., Bousahla, A.A., Tounsi, A., Alwabli, A.S., Tounsi, A. and Mahmoud, S.R. (2019), "Static analysis of laminated reinforced composite plates using a simple first-order shear deformation theory", *Comput. Concrete*, **24**(4), 369-378. https://doi.org/10.12989/cac.2019.24.4.369.

Dai, H.L., Fu, Y.M. and Dong, Z.M., (2006), "Exact solutions for functionally graded pressure vessels in a uniform magnetic field", *Int. J. Solids Struct.,* **43**, 5570-5580. https://doi.org/10.1016/j.ijsolstr.2005.08.019.

Dutta, G., Singh V.K., Mahapatra, T.R. and Panda S.K. (2017), "Electro-magneto-elastic response of laminated composite plate: A finite element approach", *Int. J. Appl. Comput. Math.*, **3**(3), 2573-2592. https://doi.org/10.1007/s40819-016-0256-6.

El-Haina, F., Bakora, A., Bousahla, A.A. and Hassan, S. (2017), "A simple analytical approach for thermal buckling of thick functionally graded sandwich plates", *Struct. Eng. Mech.*, **63**(5), 585-595. https://doi.org/10.12989/sem.2017.63.5.585.

Doan, T.N., Thom, D.V., Thanh, N.T., Chuong, P.V. and Nguyen, H.N. (2020), "Analysis of stress concentration phenomenon of cylinder laminated shells using higher-order shear deformation Quasi-3D theory", *Compos. Struct.*, **232**, 111526, https://doi.org/10.1016/j.compstruct.2019.111526.

Fang, X.Q., Liu, J.X., Yang, Sh.P. and Zhang, L.L. (2010), "Effect of surface/interface on the dynamic *stress* of two interacting *cylindrical* nano-inhomogeneities under compressional waves", *Thin Solid Films*, **518**, 6938-6944. https://doi.org/10.1016/j.tsf.2010.06.022.

Farokhian, A. (2020), "The effect of voltage and nanoparticles on the vibration of sandwich nanocomposite smart plates", *Steel Compos. Struct.,* **34**(5), 733-742. https://doi.org/10.12989/scs.2020.34.5.733.

Galic, D. and Horgan, C.O. (2002), "The stress response of radially polarized rotating piezoelectric cylinders", *J. Appl. Mech.*, **66**, 257-272. https://doi.org/10.1115/1.1572900.

Garinei, A. and Marsili, R. (2013), "Thermoelastic Stress Analysis of the contact between a flat plate and a cylinder", *Measurement*, **52**, 102-110, https://doi.org/10.1016/j.measurement.2014.03.005.

Habib, E.S., El-Hadek, M.A. and El-Megharbel, A. (2019), "Stress Analysis for Cylinder Made of FGM and Subjected to Thermo-Mechanical Loadings", *Metals*, **9**, 1-14. https://doi.org/10.3390/met9010004.

Kaddari, M., Kaci, A., Bousahla, A.A., Tounsi, A., Bourada. F., Tounsi, A., Adda Bedia, E.A. and Al-Osta, M.A. (2020), "A study on the structural behaviour of functionally graded porous plates on elastic foundation using a new quasi-3D model: Bending and free vibration analysis", *Steel Compos. Struct.,* **25**(1), 37-57. https://doi.org/10.12989/cac.2020.25.1.037.

Karami, B., Janghorban, M. and Tounsi, A. (2019), "Wave propagation of functionally graded anisotropic nanoplates resting on Winkler-Pasternak foundation", *Struct. Eng. Mech.*, **7**(1), 55-66. https://doi.org/10.12989/sem.2019.70.1.055.

Khetir, H., Bouiadjra, M.B., Houari, M.S.A., Tounsi, A. and Mahmoud, S.R. (2017), "A new nonlocal trigonometric shear deformation theory for thermal buckling analysis of embedded nanosize FG plates", *Struct. Eng. Mech.*, **64**(4), 391-402. https://doi.org/10.12989/sem.2017.64.4.391.

Lee, D.S. (2007), "The effect of an elliptic crack on the stress distribution in a long circular cylinder", *Int. J. Solids Struct.*, **44**, 4110-4119, https://doi.org/10.1016/j.ijsolstr.2006.11.009.

Li, Y., Wang, C. and Wang, R. (2012), "The thermal stress analysis and structure optimum of neck tube with vertical cryogenic insulated cylinders based on ANSYS", *Nuclear Eng. Design,* **252**, 144-152. https://doi.org/10.1016/j.nucengdes.2012.05.042.

Li, T,J,, Liu, S.W. and Chan, S.L. (2015), "Cross-sectional analysis of arbitrary sections allowing for residual stresses", *Steel Compos. Struct.*, **18**(4), 444-456, https://doi.org/10.12989/scs.2015.18.4.985.

Liew, K.M., Kitipornchai, S., Zhang, X.Z. and Lim, C.W., (2003), "Analysis of the thermal stress behaviour of functionally graded hollow circular cylinders", *Int. J. Solids Struct.,* **40**, 2355-2380, https://doi.org/10.1016/S0020-7683(03)00061-1.

Menasria, A., Bouhadra, A., Tounsi, A. and Hassan, S. (2017), "A new and simple HSDT for thermal stability analysis of FG sandwich plates", *Steel Compos. Struct.,* **25**(2), 157-175. https://doi.org/10.12989/scs.2017.25.2.157.

Mahmoudi, A., Benyoucef, S., Tounsi, A., Benachour, A., Adda Bedia, E.A. and Mahmoud, "A refined quasi-3D shear deformation theory for thermo-mechanical behavior of functionally graded sandwich plates on elastic foundations", *J. Sandw. Struct. Mat.*, **21**, 1906-1929, https://doi.org/10.1177/1099636217727577.

Medani, M., Benahmed, A., Zidour, M., Heireche, H., Tounsi, A., Bousahla, A.A., Tounsi, A. and Mahmoud, S.R. (2019), "Static and dynamic behavior of (FG-CNT) reinforced porous sandwich plate", *Steel Compos. Struct.,* **32**(5), 595-610, DOI: https://doi.org/10.12989/scs.2019.32.5.595.

Matsunaga, H. (2000), "Vibration and stability of cross-ply d composite plates according to a global higher-order plate theory", *Compos. Struct.,* **48**, 231-244.

Mehar K., Mahapatra, T.R., Panda, S.K. and Katariya, P.V. (2018), "Finite-element solution to nonlocal elasticity and scale effect on frequency behavior of shear deformable nanoplate structure", *J. Eng. Mech.,* **144**, 04018094. https://doi.org/10.1061/(ASCE)EM.1943-7889.0001519.

Mehar K. and Panda, S.K. (2019), "Multiscale modeling approach for thermal buckling analysis of nanocomposite curved structure", *Adv. Nano Res.,* **7**(3), 181-190. https://doi.org/10.12989/anr.2019.7.3.181.

Mouffoki, A., Adda Bedia, E.A., Houari M.S.A. and Hassan, S. (2017), "Vibration analysis of nonlocal advanced nanobeams in hygro-thermal environment using a new two-unknown trigonometric shear deformation beam theory", *Smart Struct. Syst.*, **20**(3), 369-383. https://doi.org/10.12989/sss.2017.20.3.369.

Motezaker, M. and Kolahchi, R. (2017), "Seismic response of CNTnanoparticles-reinforced concrete pipes based on DQ and newmark methods", *Comput. Concrete*, **19**(6), 745-753. https://doi.org/10.12989/cac.2017.19.6.745.

Noor, A.K. (1975), "Stability of multilayered composite plates", *Fibre Sci. Tech.,* **8**, 81-89.

Putcha, N.S. and Reddy, J.N. (1986), "Stability and natural vibration analysis of laminated plates by using a mixed element based on a refined plate theory", *J. Sound Vib.,* **104**, 285-300.

Reddy, J.N. (2002), *Mechanics of Laminated Composite Plates*

and Shells: Theory and Analysis, 2nd Ed., CRC Press,.

Sahla, M., Saidi, H., Draiche, K., Bousahla, A.A., Bourada, F. and Tounsi, A. (2019), "Free vibration analysis of angle-ply laminated composite and soft core sandwich plates", *Steel Compos. Struct.,* **33**(5), 663-679, DOI: https://doi.org/10.12989/scs.2019.33.5.663.

Sallem, H. and Hamdi, H. (2015), "Analysis of Measured and Predicted Residual Stresses Induced by Finish Cylindrical Grinding of High Speed Steel with CBN Wheel", *Procedia CIRP,* **31**, 381-386, https://doi.org/10.1016/j.procir.2015.03.080.

Semmah, A., Heireche, H., Bousahla, A.A. and Tounsi, A. (2019), "Thermal buckling analysis of SWBNNT on Winkler foundation by non local FSDT", *Adv. Nano Res.,* **7**(2), 89-98, https://doi.org/10.12989/anr.2019.7.2.089.

Shi, D.L. and Feng, X.Q. (2004), "The effect of nanotube waviness and agglomeration on the elastic property of carbon nanotube-reinforced composties", *J. Eng. Mat. Tech ASME*, **126**, 250-270, DOI: https://doi.org/10.1115/1.1751182

Suman, S.D., Hirwani, C.K., Chaturvedi, A. and Panda. S.K. (2017), "Effect of magnetostrictive material layer on the stress and deformation behaviour of laminated structure", IOP Conf. Series: Mat. Sci. Eng., **178** (1), 012026.

Singh V.K. and Panda S.K. (2015a), "Large amplitude free vibration analysis of laminated composite spherical shells embedded with piezoelectric layers", *Smart Struct. Syst.*, **16**(5), 853-872. https://doi.org/10.12989/sss.2015.16.5.853.

Singh V.K. and Panda S.K. (2015b), "Geometrical nonlinear free vibration analysis of laminated composite doubly curved shell panels embedded with piezoelectric layers", *J. Vib. Control*, **23**, 2078-2093. https://doi.org/10.1177/1077546315609988.

Singh V.K. and Panda S.K. (2016), "Numerical investigation on nonlinear vibration behavior of laminated cylindrical panel embedded with PZT layers", *Procedia Eng*., **144**, 660-667, https://doi.org/10.1016/j.proeng.2016.05.062.

Singh V.K., Mahapatra, T.R. and Panda S.K. (2016a), "Nonlinear transient analysis of smart laminated composite plate integrated with PVDF sensor and AFC actuator", *Compos. Struct.,* **157**, 121-130. https://doi.org/10.1016/j.compstruct.2016.08.020.

Singh V.K., Mahapatra, T.R. and Panda S.K. (2016b), "Nonlinear flexural analysis of single/doubly curved smart composite shell panels integrated with PFRC actuator", *Eur. J. Mech.-A/Solids*, **60**, 300-314, https://doi.org/10.1016/j.euromechsol.2016.08.006.

Tiersten*, H.F. (1969), "Linear piezoelectric plate vibrations*", Plenum Press, New York.

Wang, Y. and Shao, Y. (2018), "Stress analysis of a new steel-concrete composite I-girder", *Steel Compos. Struct.,* **28**(1), 51-61. https://doi.org/10.12989/scs.2018.28.1.051.

Zaoui, F.Z., Ouinas, D. and Tounsi, A. (2019), "New 2D and quasi-3D shear deformation theories for free vibration of functionally graded plates on elastic foundations", *Compos. Part B,* **159**, 231-247. https://doi.org/10.1016/j.compositesb.2018.09.051.

CC

Appendix A

$$K = K_{out}\left[1+\frac{\xi\left(\frac{K_{in}}{K_{out}}-1\right)}{1+\frac{\left(1+\frac{3K_{out}-2G_{out}}{6K_{out}+2G_{out}}\right)}{3\left(1-\frac{3K_{out}-2G_{out}}{6K_{out}+2G_{out}}\right)}(1-\xi)\left(\frac{K_{in}}{K_{out}}-1\right)}\right], \quad \text{(A1)}$$

$$G = G_{out}\left[1+\frac{\xi\left(\frac{G_{in}}{G_{out}}-1\right)}{1+\frac{2\left(4-5\frac{3K_{out}-2G_{out}}{6K_{out}+2G_{out}}\right)}{15\left(1-\frac{3K_{out}-2G_{out}}{6K_{out}+2G_{out}}\right)}(1-\xi)\left(\frac{G_{in}}{G_{out}}-1\right)}\right], \quad \text{(A2)}$$

where

$$K_{in} = K_m + \frac{\left(\delta_r - 3K_m\chi_r\right)C_r\zeta}{3\left(\xi - C_r\zeta + C_r\zeta\chi_r\right)}, \quad \text{(A3)}$$

$$K_{out} = K_m + \frac{C_r\left(\delta_r - 3K_m\chi_r\right)(1-\zeta)}{3\left[1-\xi - C_r(1-\zeta) + C_r\chi_r(1-\zeta)\right]}, \quad \text{(A4)}$$

$$G_{in} = G_m + \frac{\left(\eta_r - 3G_m\beta_r\right)C_r\zeta}{2\left(\xi - C_r\zeta + C_r\zeta\beta_r\right)}, \quad \text{(A5)}$$

$$G_{out} = G_m + \frac{C_r\left(\eta_r - 3G_m\beta_r\right)(1-\zeta)}{2\left[1-\xi - C_r(1-\zeta) + C_r\beta_r(1-\zeta)\right]}, \quad \text{(A6)}$$

where $\delta_r, \chi_r, \eta_r, \beta_r$ can be determined as

$$\chi_r = \frac{3\left(K_m + G_m\right) + k_r - l_r}{3\left(k_r + G_m\right)}, \quad \text{(A7)}$$

$$\beta_r = \frac{1}{5}\left\{\frac{4G_m + 2k_r + l_r}{3\left(k_r + G_m\right)} + \frac{4G_m}{\left(p_r + G_m\right)} + \frac{2\left[G_m\left(3K_m + G_m\right) + G_m\left(3K_m + 7G_m\right)\right]}{G_m\left(3K_m + G_m\right) + m_r\left(3K_m + 7G_m\right)}\right\}, \quad \text{(A8)}$$

$$\delta_r = \frac{1}{3}\left[n_r + 2l_r + \frac{\left(2k_r - l_r\right)\left(3K_m + 2G_m - l_r\right)}{k_r + G_m}\right], \quad \text{(A9)}$$

$$\eta_r = \frac{1}{5}\left[\frac{2}{3}\left(n_r - l_r\right) + \frac{4G_m p_r}{\left(p_r + G_m\right)} + \frac{8G_m m_r\left(3K_m + 4G_m\right)}{3K_m\left(m_r + G_m\right) + G_m\left(7m_r + G_m\right)} + \frac{2\left(k_r - l_r\right)\left(2G_m + l_r\right)}{3\left(k_r + G_m\right)}\right]. \quad \text{(A10)}$$

where, the bulk modulus (K_m) and shear modulus (G_m) o f the matrix are defined as

$$K_m = \frac{E_m}{3\left(1-2\upsilon_m\right)}, \quad \text{(A11)}$$

$$G_m = \frac{E_m}{2\left(1+\upsilon_m\right)}. \quad \text{(A12)}$$

In above relations, C_m is the volume fractions of the matrix and C_r is the the volume fractions of nanoparticles respectively and ξ and ζ describe the agglomeration of nanoparticles.

Appendix B

$$
\begin{aligned}
N_{xx} &= A_{11}\frac{\partial u}{\partial x}+A_{12}\frac{\partial v}{\partial y}+A_{16}\left(\frac{\partial u}{\partial y}+\frac{\partial v}{\partial x}\right)\\
&+B_{11}\frac{\partial \varphi_x}{\partial x}+B_{12}\frac{\partial \varphi_y}{\partial y}+B_{16}\left(\frac{\partial \varphi_x}{\partial y}+\frac{\partial \varphi_y}{\partial x}\right)\\
&+E_{11}c_1\left(\frac{\partial \varphi_x}{\partial x}+\frac{\partial^2 w}{\partial x^2}\right)+E_{12}c_1\left(\frac{\partial \varphi_y}{\partial y}+\frac{\partial^2 w}{\partial y^2}\right)\\
&+E_{16}c_1\left(\frac{\partial \varphi_y}{\partial x}+\frac{\partial \varphi_x}{\partial y}+2\frac{\partial^2 w}{\partial x\,\partial y}\right),\\
N_{yy} &= A_{12}\frac{\partial u}{\partial x}+A_{22}\frac{\partial v}{\partial y}+A_{26}\left(\frac{\partial u}{\partial y}+\frac{\partial v}{\partial x}\right)\\
&+B_{12}\frac{\partial \varphi_x}{\partial x}+B_{22}\frac{\partial \varphi_y}{\partial y}+B_{26}\left(\frac{\partial \varphi_x}{\partial y}+\frac{\partial \varphi_y}{\partial x}\right)\\
&+E_{12}c_1\left(\frac{\partial \varphi_x}{\partial x}+\frac{\partial^2 w}{\partial x^2}\right)+E_{22}c_1\left(\frac{\partial \varphi_y}{\partial y}+\frac{\partial^2 w}{\partial y^2}\right)\\
&+E_{26}c_1\left(\frac{\partial \varphi_y}{\partial x}+\frac{\partial \varphi_x}{\partial y}+2\frac{\partial^2 w}{\partial x\,\partial y}\right),\\
N_{xy} &= A_{16}\frac{\partial u}{\partial x}+A_{26}\frac{\partial v}{\partial y}+A_{66}\left(\frac{\partial u}{\partial y}+\frac{\partial v}{\partial x}\right)\\
&+B_{16}\frac{\partial \varphi_x}{\partial x}+B_{26}\frac{\partial \varphi_y}{\partial y}+B_{66}\left(\frac{\partial \varphi_x}{\partial y}+\frac{\partial \varphi_y}{\partial x}\right)\\
&+E_{16}c_1\left(\frac{\partial \varphi_x}{\partial x}+\frac{\partial^2 w}{\partial x^2}\right)+E_{26}c_1\left(\frac{\partial \varphi_y}{\partial y}+\frac{\partial^2 w}{\partial y^2}\right)\\
&+E_{66}c_1\left(\frac{\partial \varphi_y}{\partial x}+\frac{\partial \varphi_x}{\partial y}+2\frac{\partial^2 w}{\partial x\,\partial y}\right),
\end{aligned}
\tag{B1}
$$

$$
\begin{aligned}
M_{xx} &= B_{11}\frac{\partial u}{\partial x}+B_{12}\frac{\partial v}{\partial y}+B_{16}\left(\frac{\partial u}{\partial y}+\frac{\partial v}{\partial x}\right)\\
&+D_{11}\frac{\partial \varphi_x}{\partial x}+D_{12}\frac{\partial \varphi_y}{\partial y}+D_{16}\left(\frac{\partial \varphi_x}{\partial y}+\frac{\partial \varphi_y}{\partial x}\right)\\
&+F_{11}c_1\left(\frac{\partial \varphi_x}{\partial x}+\frac{\partial^2 w}{\partial x^2}\right)+F_{12}c_1\left(\frac{\partial \varphi_y}{\partial y}+\frac{\partial^2 w}{\partial y^2}\right)\\
&+F_{16}c_1\left(\frac{\partial \varphi_y}{\partial x}+\frac{\partial \varphi_x}{\partial y}+2\frac{\partial^2 w}{\partial x\,\partial y}\right),\\
M_{yy} &= B_{12}\frac{\partial u}{\partial x}+B_{22}\frac{\partial v}{\partial y}+B_{26}\left(\frac{\partial u}{\partial y}+\frac{\partial v}{\partial x}\right)\\
&+D_{12}\frac{\partial \varphi_x}{\partial x}+D_{22}\frac{\partial \varphi_y}{\partial y}+D_{26}\left(\frac{\partial \varphi_x}{\partial y}+\frac{\partial \varphi_y}{\partial x}\right)\\
&+F_{12}c_1\left(\frac{\partial \varphi_x}{\partial x}+\frac{\partial^2 w}{\partial x^2}\right)+F_{22}c_1\left(\frac{\partial \varphi_y}{\partial y}+\frac{\partial^2 w}{\partial y^2}\right)\\
&+F_{26}c_1\left(\frac{\partial \varphi_y}{\partial x}+\frac{\partial \varphi_x}{\partial y}+2\frac{\partial^2 w}{\partial x\,\partial y}\right),\\
M_{xy} &= B_{16}\frac{\partial u}{\partial x}+B_{26}\frac{\partial v}{\partial y}+B_{66}\left(\frac{\partial u}{\partial y}+\frac{\partial v}{\partial x}\right)\\
&+D_{16}\frac{\partial \varphi_x}{\partial x}+D_{26}\frac{\partial \varphi_y}{\partial y}+D_{66}\left(\frac{\partial \varphi_x}{\partial y}+\frac{\partial \varphi_y}{\partial x}\right)\\
&+F_{16}c_1\left(\frac{\partial \varphi_x}{\partial x}+\frac{\partial^2 w}{\partial x^2}\right)+F_{26}c_1\left(\frac{\partial \varphi_y}{\partial y}+\frac{\partial^2 w}{\partial y^2}\right)\\
&+F_{66}c_1\left(\frac{\partial \varphi_y}{\partial x}+\frac{\partial \varphi_x}{\partial y}+2\frac{\partial^2 w}{\partial x\,\partial y}\right),
\end{aligned}
\tag{B2}
$$

$$
\begin{aligned}
P_{xx} &= E_{11}\frac{\partial u}{\partial x}+E_{12}\frac{\partial v}{\partial y}+E_{16}\left(\frac{\partial u}{\partial y}+\frac{\partial v}{\partial x}\right)\\
&+F_{11}\frac{\partial \varphi_x}{\partial x}+F_{12}\frac{\partial \varphi_y}{\partial y}+F_{16}\left(\frac{\partial \varphi_x}{\partial y}+\frac{\partial \varphi_y}{\partial x}\right)\\
&+H_{11}c_1\left(\frac{\partial \varphi_x}{\partial x}+\frac{\partial^2 w}{\partial x^2}\right)+H_{12}c_1\left(\frac{\partial \varphi_y}{\partial y}+\frac{\partial^2 w}{\partial y^2}\right)\\
&+H_{16}c_1\left(\frac{\partial \varphi_y}{\partial x}+\frac{\partial \varphi_x}{\partial y}+2\frac{\partial^2 w}{\partial x\,\partial y}\right),\\
P_{yy} &= E_{12}\frac{\partial u}{\partial x}+E_{22}\frac{\partial v}{\partial y}+E_{26}\left(\frac{\partial u}{\partial y}+\frac{\partial v}{\partial x}\right)\\
&+F_{12}\frac{\partial \varphi_x}{\partial x}+F_{22}\frac{\partial \varphi_y}{\partial y}+F_{26}\left(\frac{\partial \varphi_x}{\partial y}+\frac{\partial \varphi_y}{\partial x}\right)\\
&+H_{12}c_1\left(\frac{\partial \varphi_x}{\partial x}+\frac{\partial^2 w}{\partial x^2}\right)+H_{22}c_1\left(\frac{\partial \varphi_y}{\partial y}+\frac{\partial^2 w}{\partial y^2}\right)\\
&+H_{26}c_1\left(\frac{\partial \varphi_y}{\partial x}+\frac{\partial \varphi_x}{\partial y}+2\frac{\partial^2 w}{\partial x\,\partial y}\right),\\
P_{xy} &= E_{16}\frac{\partial u}{\partial x}+E_{26}\frac{\partial v}{\partial y}+E_{66}\left(\frac{\partial u}{\partial y}+\frac{\partial v}{\partial x}\right)\\
&+F_{16}\frac{\partial \varphi_x}{\partial x}+F_{26}\frac{\partial \varphi_y}{\partial y}+F_{66}\left(\frac{\partial \varphi_x}{\partial y}+\frac{\partial \varphi_y}{\partial x}\right)\\
&+H_{16}c_1\left(\frac{\partial \varphi_x}{\partial x}+\frac{\partial^2 w}{\partial x^2}\right)+H_{26}c_1\left(\frac{\partial \varphi_y}{\partial y}+\frac{\partial^2 w}{\partial y^2}\right)\\
&+H_{66}c_1\left(\frac{\partial \varphi_y}{\partial x}+\frac{\partial \varphi_x}{\partial y}+2\frac{\partial^2 w}{\partial x\,\partial y}\right),
\end{aligned}
\tag{B3}
$$

$$
\begin{aligned}
Q_{xx} &= A_{55}\left(\frac{\partial w}{\partial x}+\varphi_x\right)+A_{45}\left(\frac{\partial w}{\partial y}+\varphi_y\right)\\
&+D_{55}c_2\left(\varphi_x+\frac{\partial w}{\partial x}\right)+D_{45}c_2\left(\frac{\partial w}{\partial y}+\varphi_y\right),\\
Q_{yy} &= A_{45}\left(\frac{\partial w}{\partial y}+\varphi_y\right)+A_{44}\left(\frac{\partial w}{\partial y}+\varphi_y\right)\\
&+D_{45}c_2\left(\varphi_y+\frac{\partial w}{\partial y}\right)+D_{44}c_2\left(\frac{\partial w}{\partial y}+\varphi_y\right),
\end{aligned}
\tag{B4}
$$

$$
\begin{aligned}
K_{xx} &= D_{55}\left(\varphi_x+\frac{\partial w}{\partial x}\right)+D_{45}\left(\varphi_y+\frac{\partial w}{\partial y}\right)+\\
&F_{55}c_2\left(\varphi_x+\frac{\partial w}{\partial x}\right)+F_{45}c_2\left(\varphi_y+\frac{\partial w}{\partial y}\right)\\
K_{yy} &= D_{45}\left(\varphi_x+\frac{\partial w}{\partial x}\right)+D_{44}\left(\varphi_y+\frac{\partial w}{\partial y}\right)\\
&+F_{45}c_2\left(\varphi_x+\frac{\partial w}{\partial x}\right)\\
&+F_{44}c_2\left(\varphi_y+\frac{\partial w}{\partial y}\right)
\end{aligned}
\tag{B5}
$$

where

$$A_{ij} = \left[\int_{-h_c/2}^{h_c/2} Q_{11} z\, dz + \int_{-h_c/2}^{h_c/2+h_p} C_{11} z\, dz \right], \qquad \text{(B6)}$$

$$B_{ij} = \left[\int_{-h_c/2}^{h_c/2} Q_{11} z^2 dz + \int_{-h_c/2}^{h_c/2+h_p} C_{11} z^2\, dz \right], \qquad \text{(B7)}$$

$$D_{ij} = \left[\int_{-h_c/2}^{h_c/2} Q_{11} z^2 dz + \int_{-h_c/2}^{h_c/2+h_p} C_{11} z^2\, dz \right], \qquad \text{(B8)}$$

$$E_{ij} = \left[\int_{-h_c/2}^{h_c/2} Q_{11} z^3 dz + \int_{-h_c/2}^{h_c/2+h_p} C_{11} z^3\, dz \right], \qquad \text{(B9)}$$

$$F_{ij} = \left[\int_{-h_c/2}^{h_c/2} Q_{11} z^4 dz + \int_{-h_c/2}^{h_c/2+h_p} C_{11} z^4\, dz \right], \qquad \text{(B10)}$$

$$H_{ij} = \left[\int_{-h_c/2}^{h_c/2} Q_{11} z^6 dz + \int_{-h_c/2}^{h_c/2+h_p} C_{11} z^6\, dz \right], \qquad \text{(B11)}$$